Available online at www.sciencedirect.com
SCIENCE DIRECT®

Journal of the European Ceramic Society 23 (2003) 2503–2506

www.elsevier.com/locate/jeurceramsoc

The relationship between microstructure and quality factor for $(Al,Mg,Ta)O_2$ microwave dielectrics

Ji-Won Choi[a,*], Hwack-Joo Lee[b], Seok-Jin Yoon[a], Hyun-Jai Kim[a], Ki Hyun Yoon[c]

[a]*Thin Film Technology Research Center, Korea Institute of Science and Technology, Seoul 130-650, South Korea*
[b]*New Materials Evaluation Center, Korea Research Institute of Standard and Science, Taejon 305-600, South Korea*
[c]*Department of Ceramic Engineering, Yonsei University, Seoul 120-749, South Korea*

Abstract

The relationship between microstructures and quality factor (Q) of $(1-x)(Al_{1/2}Ta_{1/2})O_2$–$x(Mg_{1/3}Ta_{2/3})O_2$ ceramics was investigated. The extrinsic loss of microwave dielectrics depended on cations ordering, grain size, and porosity. $(Al_{1/2}Ta_{1/2})O_2$ has a disordered structure and $(Mg_{1/3}Ta_{2/3})O_2$ has an ordered trirutile structure. As $(Mg_{1/3}Ta_{2/3})O_2$ content increased, $(1-x)(Al_{1/2}Ta_{1/2})O_2$–$x(Mg_{1/3}Ta_{2/3})O_2$ ceramics revealed an ordered phase and were of single phase for $x>0.6$. The increase of the ordered phase and grain size enhanced the Q. When ordering was completed at $(Mg_{1/3}Ta_{2/3})O_2$ concentration over 60 mol%, the grain size was a major factor in the increase the Q value. In contrast the porosity degraded the Q value. Therefore, the Q value depended on order/disorder, the porosity, and the grain size in that order.

Keywords: Grain size; Microstructure; Microwave ceramics; Ordering; Quality factor; $(Al,Mg,Ta)O_2$

1. Introduction

Microwave dielectric materials have to exhibit dielectric characteristics[1–3] such as high dielectric constant (ε_r), high quality factor (Q), and stable ($\approx$0 ppm/°C) temperature coefficient of the resonant frequency (τ_f). Among these requirements, the dielectric constant and the temperature coefficient of resonant frequency depend on composition and the dielectric loss depends on intrinsic loss by phonon, and extrinsic loss depends on factors such as porosity, grain size, impurity, defects, and so on.

There are competing theories about the Q factor. Davis et al.[4] reported that the ordering is important factor to enhance the Q factor in the $Ba(Zn_{1/3}Ta_{2/3})O_3$–$BaZrO_3$ system. On the other hand, Nahm et al.[5] reported that the grain size is the main factor to enhance the Q factor, with no dependence on the ordering in the $Ba(Zn_{1/3}Ta_{2/3})O_3$ system with ZrO_2.

The purpose of present work is to establish the extrinsic dielectric loss mechanism for $(1-x)(Al_{1/2}Ta_{1/2})O_2$–$x(Mg_{1/3}Ta_{2/3})O_2$ ceramics based upon microstructures obtained by scanning electron microscopy (SEM) and transmission electron microscopy (TEM). The effects of order/disorder, grain size, and porosity on the Q factor are discussed.

2. Experimental procedure

$(1-x)(Al_{1/2}Ta_{1/2})O_2$–$x(Mg_{1/3}Ta_{2/3})O_2$ ($0\leqslant x\leqslant 1.0$) powder compositions were synthesized using the conventional solid-state reaction method. The starting materials were Al_2O_3 (Aldrich, 99.7%), Ta_2O_5 (Aldrich, 99%), and MgO (Aldrich, 98%). Stoichiometric compositions were mixed for 24 h with stabilized ZrO_2 media and distilled water, then dried and calcined. The calcined powders were re-milled and pressed into rods of 12 mm diameter and 6 mm thickness under a pressure of 150 MPa. The pellets were sintered at 1450 °C for 3 h in air, and the sintered specimens were polished to precise dimensions to achieve the ratio of thickness to diameter of 0.4–0.5.

X-ray diffractometry (XRD, CuK_α radiation, Model Rint/Dmax 2500, Rigaku, Japan) was conducted on powders obtained by crushing the sintered specimens for phase identification and lattice parameter measurements. The bulk densities of the sintered pellets were determined by the Archimedes method. The microstructures of the sintered specimens were investigated using SEM

* Corresponding author.

0955-2219/03/$ - see front matter © 2003 Elsevier Ltd. All rights reserved.
doi:10.1016/S0955-2219(03)00169-9

and TEM. The polished surfaces of the ceramics were investigated by scanning electron microscopy (SEM, Model S-4200, Hitachi, Japan) after thermal etching at 1380 °C for 20 min in air. The TEM specimens were prepared by ultrasonic cutting 3 mm diameter disks and mechanical polishing them to a thickness of ~100 μm. The central parts of the disks were further reduced to ~10 μm by mechanical dimpling followed by final polishing. The final perforation of the specimen was conducted by precision argon-ion milling (Model 691 Gatan, San Francisco, CA) with an acceleration voltage of 3 KeV. These specimens were examined using a side-entry-type high resolution TEM (Model H9000-NAR, Hitachi, Kastsuda, Ibaraki, Japan) operated at 300 kV with a point resolution of 0.18 nm. The SAED (selected area electron diffractometry) and BF-TEM (bright field TEM) images could be obtained. The dielectric loss was measured at 6–11 GHz using the parallel-plate (Hakki and Coleman) method interfaced with a network analyzer (HP-8720C, Hewlett Packard, USA).[6]

3. Results and discussion

Fig. 1 shows powder X-ray diffraction patterns for $(1-x)(Al_{1/2}Ta_{1/2})O_2$–$x(Mg_{1/3}Ta_{2/3})O_2$ ceramics sintered at 1450 °C for 3 h. $(Al_{1/2}Ta_{1/2})O_2$ is orthorhombic single phase and $(Mg_{1/3}Ta_{2/3})O_2$ is tetragonal single phase. In the case of $(Mg_{1/3}Ta_{2/3})O_2$ concentrations under 40 mol%, $(1-x)(Al_{1/2}Ta_{1/2})O_2$–$x(Mg_{1/3}Ta_{2/3})O_2$ ceramics have mixed phase. As $(Mg_{1/3}Ta_{2/3})O_2$ concentration increased to over 60 mol%, $(1-x)(Al_{1/2}Ta_{1/2})O_2$–$x(Mg_{1/3}Ta_{2/3})O_2$ transformed into tetragonal structure.

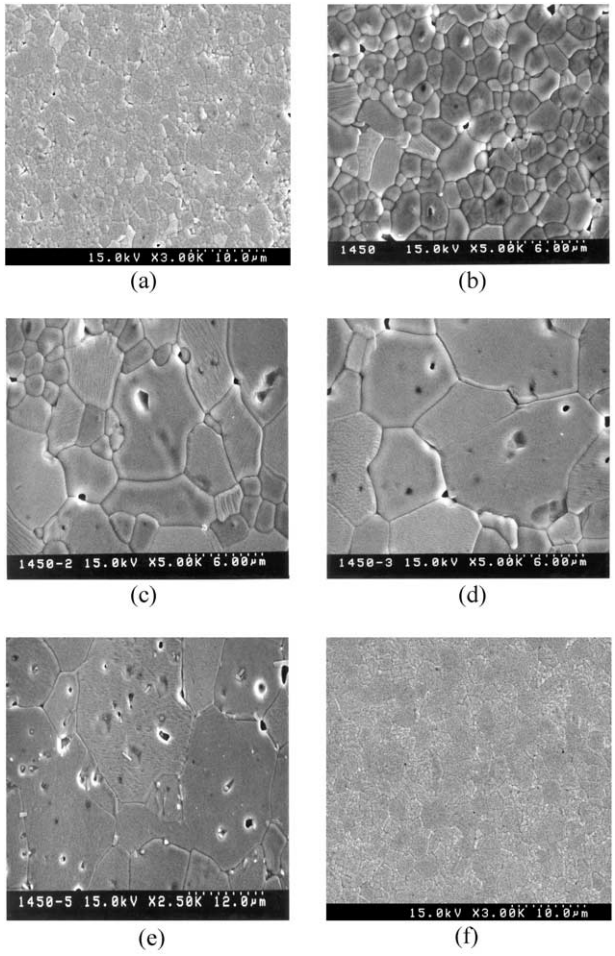

Fig. 2. SEM photographs of $(1-x)(Al_{1/2}Ta_{1/2})O_2$–$x(Mg_{1/3}Ta_{2/3})O_2$ ceramics sintered at 1450 °C for 3 h: (a) $x=0$, (b) $x=0.2$, (c) $x=0.4$, (d) $x=0.6$, (e) $x=0.8$, (f) $x=1.0$.

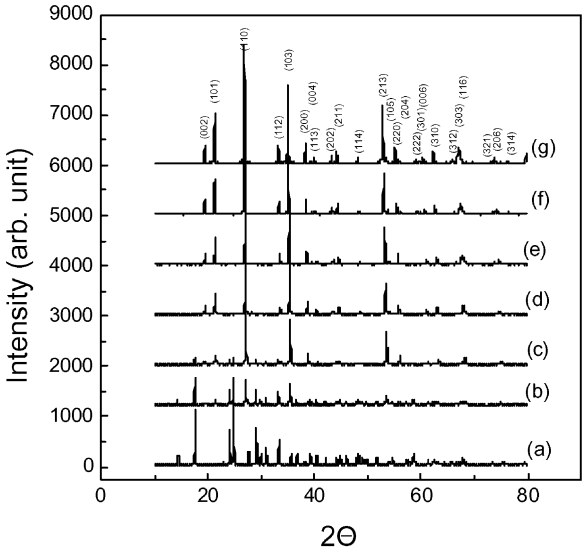

Fig. 1. X-ray diffraction patterns of $(1-x)(Al_{1/2}Ta_{1/2})O_2$–$x(Mg_{1/3}Ta_{2/3})O_2$ ceramics sintered at 1450 °C for 3 h: (a) $x=0$, (b) $x=0.2$, (c) $x=0.4$, (d) $x=0.6$, (e) $x=0.65$, (f) $x=0.8$, (g) $x=1.0$.

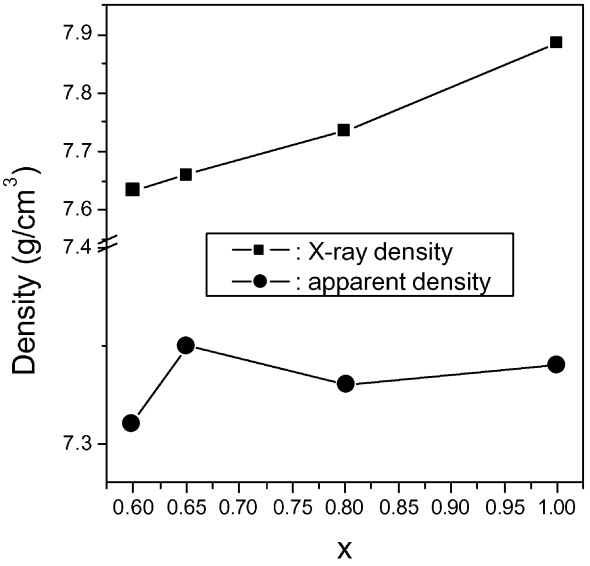

Fig. 3. Densities for $(1-x)(Al_{1/2}Ta_{1/2})O_2$–$x(Mg_{1/3}Ta_{2/3})O_2$ ceramics sintered at 1450 °C for 3 h.

Fig. 2 shows SEM photographs of $(1-x)(Al_{1/2}Ta_{1/2})O_2$–$x(Mg_{1/3}Ta_{2/3})O_2$ ceramics sintered at 1450 °C for 3 h. It is necessary to note that the SEM photographs have different magnifications for convenience. $(Al_{1/2}Ta_{1/2})O_2$ [Fig. 2(a)] has a small grain size. As the $(Mg_{1/3}Ta_{2/3})O_2$ concentration increases from 20 to 65 mol%, the grain size increases from 2 to 12 μm and porosity decreases. When $(Mg_{1/3}Ta_{2/3})O_2$ concentration is 80 mol%, however, the grain size is significantly large (15 μm) and the pore size inside the grains is also large. The decrease of apparent density at $(Mg_{1/3}Ta_{2/3})O_2$ concentration of 80 mol% stems from these increase of porosity as shown in Fig. 3. It is an interesting result that $(Mg_{1/3}Ta_{2/3})O_2$ [Fig. 2(f)] has small grain size.

Fig. 4 shows the SAED patterns for $(1-x)(Al_{1/2}Ta_{1/2})O_2$–$x(Mg_{1/3}Ta_{2/3})O_2$ ceramics sintered at 1450 °C for 3 h. $(Al_{1/2}Ta_{1/2})O_2$ [Fig. 4(a)] does not show any ordered phase. $(Mg_{1/3}Ta_{2/3})O_2$ [Fig. 4(e)] shows 1:2 ordered trirutile structure. As $(Mg_{1/3}Ta_{2/3})O_2$ concentration increased from 20 to 40 mol%, the ordered phase starts to appear and is mixed with disordered one. In the case of $(Mg_{1/3}Ta_{2/3})O_2$ concentration over 60 mol%, $(1-x)(Al_{1/2}Ta_{1/2})O_2$–$x(Mg_{1/3}Ta_{2/3})O_2$ ceramics shows fully 1:2 ordered phase.

Fig. 5 shows the BF-TEM images for $(1-x)(Al_{1/2}Ta_{1/2})O_2$–$x(Mg_{1/3}Ta_{2/3})O_2$ ceramics sintered at 1450 °C for 3 h. These images agree with SAED patterns shown in Fig. 4. $(Al_{1/2}Ta_{1/2})O_2$ [Fig. 5(a)] does not show any APBs (anti-phase boundaries).[7] This means $(Al_{1/2}Ta_{1/2})O_2$ is not an ordered phase. $(Mg_{1/3}Ta_{2/3})O_2$ [Fig. 5(e)] shows APBs. As the $(Mg_{1/3}Ta_{2/3})O_2$ concentration increases from 20 to 40 mol%, the APBs start to appear and when $(Mg_{1/3}Ta_{2/3})O_2$ concentration is 60 mol%, $(1-x)(Al_{1/2}Ta_{1/2})O_2$–$x(Mg_{1/3}Ta_{2/3})O_2$ ceramics show many APBs.

Fig. 6 shows the $Q \cdot f_0$ variation for $(1-x)(Al_{1/2}Ta_{1/2})O_2$–$x(Mg_{1/3}Ta_{2/3})O_2$ ceramics sintered at 1450 °C for 3 h. As $(Mg_{1/3}Ta_{2/3})O_2$ concentration increased from 0 to 65

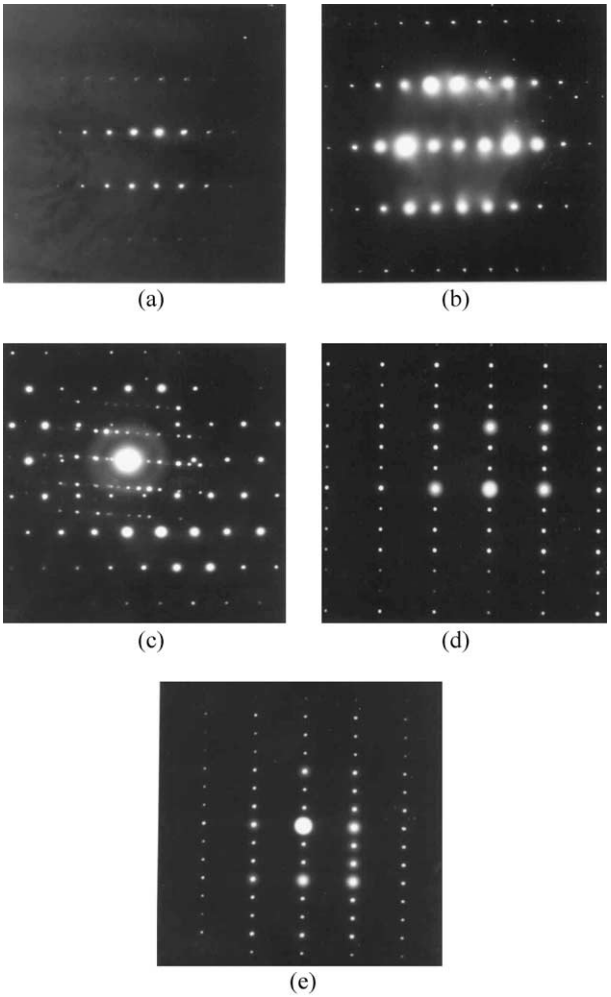

Fig. 4. SAED patterns of $(1-x)(Al_{1/2}Ta_{1/2})O_2$–$x(Mg_{1/3}Ta_{2/3})O_2$ ceramics sintered at 1450 °C for 3 h: (a) $x=0$ with [001] zone axes, (b) $x=0.2$ with [001] zone axes, (c) $x=0.4$, (d) $x=0.6$ with [110] zone axes, (e) $x=1.0$ with [110] zone axes.

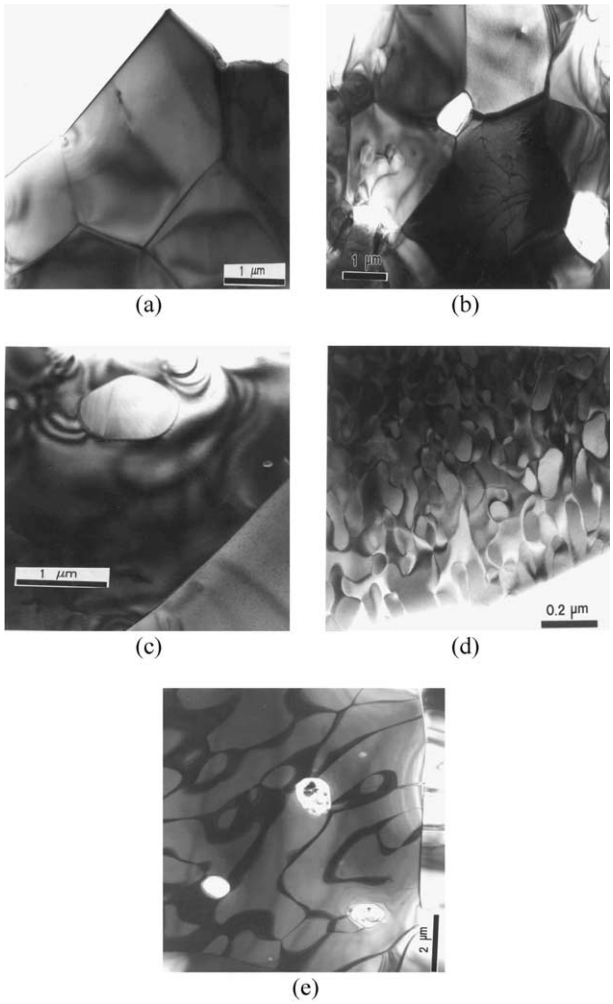

Fig. 5. BF-TEM images of $(1-x)(Al_{1/2}Ta_{1/2})O_2$–$x(Mg_{1/3}Ta_{2/3})O_2$ ceramics sintered at 1450 °C for 3 h: (a) $x=0$, (b) $x=0.2$, (c) $x=0.4$, (d) $x=0.6$, (e) $x=1.0$.

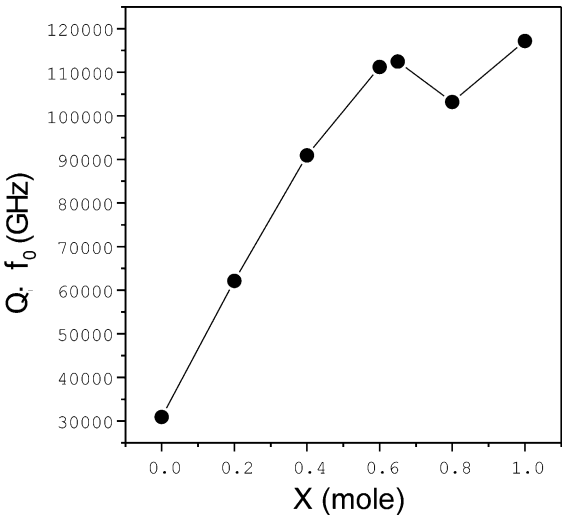

Fig. 6. $Q{\cdot}f_0$ value of $(1-x)(Al_{1/2}Ta_{1/2})O_2$–$x(Mg_{1/3}Ta_{2/3})O_2$ ceramics sintered at 1450 °C for 3 h.

mol%, the $Q{\cdot}f_0$ linearly increases from 30,900 to 112,500 GHz, and slightly decreases to 103,200 GHz at 80 mol% and then increases again to 117,200 GHz at 100 mol%. The variation of $Q{\cdot}f_0$ can be explained by microstructures. As shown in Figs. 4(a), (e) and 5(a), (e), $(Al_{1/2}Ta_{1/2})O_2$ is not ordered and $(Mg_{1/3}Ta_{2/3})O_2$ has an 1:2 ordered trirutile structure. These compositions have small grain size and porosity in comparison with $(Al_{1/2}Ta_{1/2})O_2$–$(Mg_{1/3}Ta_{2/3})O_2$ compounds shown in SEM photographs [Fig. 2(b)–(e)]. The large difference of $Q{\cdot}f_0$ between $(Al_{1/2}Ta_{1/2})O_2$ (30,900 GHz) and $(Mg_{1/3}Ta_{2/3})O_2$ (117,200 GHz) is not generated from grain size or porosity but is due to cation ordering. On the other hand, Fig. 6 can be divided into two regions which are 0–60 and 60–100 mol%. As $(Mg_{1/3}Ta_{2/3})O_2$ concentration increases from 0 to 60 mol%, the $Q{\cdot}f_0$ linearly increases, and the ordering started from 20 mol% and completed at 60 mol% shown in Figs. 4(b)–(d) and 5(b)–(d). Of course, the grain size also rapidly increases in the region. As $(Mg_{1/3}Ta_{2/3})O_2$ concentration increases from 60 to 100 mol%, the $Q{\cdot}f_0$ varies, with both increase and decrease but the $Q{\cdot}f_0$ variation is small. The ordering state is nearly the same as shown in Fig. 4(d)–(e) but the grain size also increases rapidly in the region. The decrease of $Q{\cdot}f_0$ at 80 mol% is due to the increase of porosity in the grains. From these results, the variation of $Q{\cdot}f_0$ due to ordering is dominant. However the variation of $Q{\cdot}f_0$ due to grain size is not so large as ordering and when the porosity in the grains increases, the $Q{\cdot}f_0$ decreases though the grain size increases. Therefore, the main factor, which affects the $Q{\cdot}f_0$, is cation order/disorder. The grain size is of secondary importance factor and $Q{\cdot}f_0$ depends on not only the grain size but also the porosity in the grains.

4. Conclusions

The relationship between microstructures and quality factor (Q) of $(1-x)(Al_{1/2}Ta_{1/2})O_2$–$x(Mg_{1/3}Ta_{2/3})O_2$ ceramics was investigated. The extrinsic loss of microwave dielectrics depended on cation ordering, grain size, and porosity. The high $Q{\cdot}f_0$ difference between $(Al_{1/2}Ta_{1/2})O_2$ (30,900 GHz) and $(Mg_{1/3}Ta_{2/3})O_2$ (117,200 GHz) was not because of grain size or porosity but due to ordering. The variations of $Q{\cdot}f_0$ due to ordering is very large. However, changes in $Q{\cdot}f_0$ due to grain size is not large when the porosity in the grains increase, the $Q{\cdot}f_0$ decreases though the grain size increases. Therefore, the main factor controlling the $Q{\cdot}f_0$ is cation order/disorde; the grain size is secondary importance factor and $Q{\cdot}f_0$ depends on not only the grain size but also the porosity in the grains.

References

1. Wersing, W., High Frequency ceramic dielectrics and their application for microwave components. In *Electronic Ceramics*, ed. B. C. H. Steele. Elsevier Applied Science, London, UK, 1991, pp. 67–119.
2. Nomura, S., Ceramics for microwave dielectric resonator. *Ferroelectrics*, 1983, **49**, 61–70.
3. O'Bryan, H. M., Thomson Jr., J. and Plourde, J. K., A new BaO–TiO_2 compound with temperature stable high permittivity and low loss. *J. Am Ceram. Soc.*, 1974, **57**, 450.
4. Davies, P. K., Tong, J. and Negas, T., Effect of ordering-induced domain boundaries on low-loss $Ba(Zn_{1/3}Ta_{2/3})O_3$–$BaZrO_3$ perovskite microwave dielectrics. *J. Am. Ceram. Soc.*, 1997, **80**(7), 1727–1740.
5. Yang, J. I., Nahm, S., Choi, C. H., Lee, H. J. and Park, H. M., Microstructure and microwave dielectric properties of $Ba(Zn_{1/3}Ta_{2/3})O_3$ ceramics with ZrO_2 addition. *J. Am. Ceram. Soc.*, 2002, **85**(1), 165–168.
6. Hakki, B. W. and Coleman, P. D., A dielectric resonator method of measuring inductive capacities in the millimeter range. *IRE Transaction Microwave Theory & Technology*, 1960, **8**, 402–410.
7. Lee, H. J., Park, H. M., Cho, Y. K., Song, Y. W., Nahm, S. and Byun, J. D., Microstructure characterizations in calcium magnesium niobate. *J. Am. Ceram. Soc.*, 2001, **84**(7), 1632–1636.